ATLAS NOTE

September 19, 2014

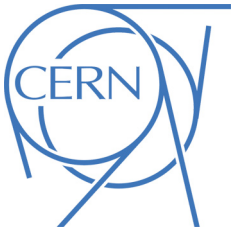

Lepton Isolation Using Particle Flow Objects for the ATLAS Detector

Seth Moortgat[a,b]

[a]*Master Student Physics and Astronomy Vrije Universiteit Brussel, Belgium*
[b]*CERN Summer Student under the supervision of Heather Gray and Andreas Salzburger, further assisted by Christopher Young and the Particle Flow group for ATLAS*

Abstract

This note presents a novel method for isolation using particle flow objects. The study is focused on muon isolation, but it is expected that these techniques would also be applicable for electrons and photons. It will be shown to be robust against pile-up, which is one of the challenges at the LHC. Above that, high efficiency in identifying truly isolated particles needs to be balanced by good fake rejection such that non-isolated particles do not pass the isolation criteria. Particle flow isolation shows improvements over previously used track and calorimeter based isolation, preserving a higher fake rejection for a similar isolation efficiency. For an efficiency of 90%, particle flow isolation achieves a fake rejection of 63% whereas the standard isolation techniques reach only 40%.

Contents

Introduction

The LHC [10] is currently the most powerful particle accelerator in the world, producing proton-proton collisions at center of mass energies of 7 and 8 TeV, respectively in 2012 and 2013 and expected to deliver collisions at an energy of around 13 TeV in 2015. ATLAS [2] is one of two general purpose detectors located at one of eight interaction points, where each 25 ns proton bunches are made to collide and produce many particles to be detected. Most interactions between the partons are soft scattering processes and do not produce new interesting physics phenomena. However when two partons collide directly (also called the hard scatter event), they liberate significant energy which can be used to produce new particles. In order to study these potentially interesting events, the prompt hard scatter decay products must be identified. Therefore the concept of isolation has been introduced. Promptly produced particles from the hard scatter tend to be isolated, whereas similar particles from jets or soft scatter events tend to have a lot of energy surrounding them. However, it can be that interesting physics is hidden within other phenomena, especially when the objects of interest are highly boosted, and isolation might not always be the best way to approach such an analysis (see for example [5]).

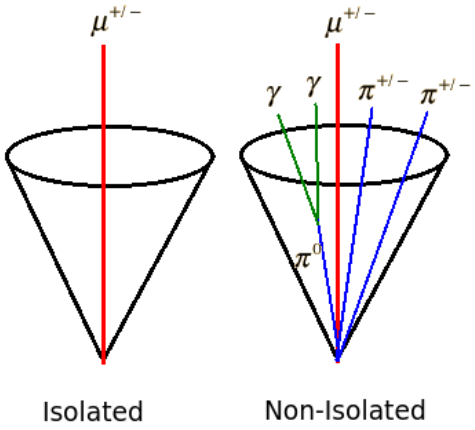

Figure 1: Illustration of and isolated muon on the left and a non-isolated muon on the right.

Isolation Isolation ($\mathfrak{I}$) uses the amount of energy surrounding the particle of interest to determine whether the particle is prompt or not. This surrounding energy can be either from charged or neutral particles[1]. Isolation is expressed as the sum of the p_T of all the particles which lie within a certain isolation cone around the particle of interest, as expressed in equation 1.

$$\mathfrak{I} = \sum p_T(\in cone) \tag{1}$$

If there is a lot of energy inside the isolation cone, the particle is very likely created in a jet together with a lot of other particles surrounding it, whereas a hard scatter prompt decay product will have almost no energy surrounding it. This is illustrated in figure 1.
New physics phenomena can only be discovered when the interesting hard scatter events are identified, which is why isolation has proven to be of great importance in these searches. Isolation is badly influenced by pile-up events and it relies heavily on the reconstruction of all the particles inside the detector. This is why particle flow might improve the isolation performance.

Pile-Up As proton bunches collide inside the detector there are not just two single partons colliding, but up to about 30 interactions occur between the partons (quarks and gluons) inside the protons rather than between the protons as a whole. This gives rise to multiple interaction vertices for each bunch crossing, most of which are caused by low energy events that can be identified by the presence of additional reconstructed vertices. Usually only one of the vertices[2] arises from a hard scatter event and is the

[1]For charged particles we usually work in terms of p_T, whereas for neutral particles more often E_T is used. In the end they can be easily related to one another by the expression (in natural units): $E^2 = m^2 + p^2$ and for low mass particles with relatively high momentum, E_T and p_T are very similar. Throughout this note p_T will be used when it concerns particle flow (although it may include charged and neutral particles) or track based isolation and only when isolation based on calorimeter cells is discussed, E_T will appear.

[2]Most of the time there will be even no hard scatter events, but these events would probably not pass the trigger and would be thrown away.

one of interest. All the other vertices are considered in-time pile-up. Closely related is the out-of-time pile-up. This is caused by signals from the previous bunch crossing, who are mixed with the current bunch crossing signals since it takes some time for the detector to read out the electronics[3]. Pile-up is distinguished from the underlying event which is caused by the remaining partons inside a colliding proton which did not partake in the hard scatter event but which may produce extra energy within the isolation cone.
Pile-up is one of the biggest issues for isolation. As will be discussed in more detail later, the isolation of a particle is measured using an isolation cone in the $\eta - \phi$ plane, collecting every particle which is close to the particle of interest in η and ϕ (see section 2 for a clear definition of the isolation cone). Pile-up particles, although originating from another vertex, may also be close in η and ϕ and may contaminate the isolation cone but have been produced at a distance from the particle of interest. In section 3 the subtraction of pile-up from the isolation cone will be discussed for both charged and neutral particles.

Particle Flow The particle flow (also p-flow) algorithm [6] aims at reconstructing all stable particles inside the detector. These include electrons, photons, muons, charged and neutral hadrons (being mostly pions, kaons, and neutrons). Particle flow algorithms combine and link all detector parts (inner detector, calorimeter systems and muon systems), thereby improving the resolution on the energy, momentum and direction of all these particles. This has been studied and proven to give better resolutions in comparison to only using tracks, calorimeter clusters or hits in the muon system separately.

The particle flow reconstruction algorithm is performed in three stages. First the different basic elements are reconstructed. This consists of an iterative tracking algorithm to find all the tracks in the tracker, a clustering algorithm using the calorimeter information (both electromagnetic and hadronic) and searching for tracks in the muon system. These are all standard ATLAS reconstruction techniques and are not part of the new particle flow algorithm. Then associations are made between the different objects from different detector parts. In the final step the true particle flow algorithm tries to further refine these associations in order to identify the final particles.

In the first step, the standard reconstruction algorithms are applied to the separate detector elements. An iterative tracking algorithm aims at high tracking efficiency with a low fake rate. This is achieved by first applying very tight criteria to the tracks in the first iterations, making sure almost no fakes are included, but with low efficiency. Hits from the tracks that are found are removed, which lowers the possibility to have fakes (fewer hits means fewer chance on combining them by accident into a fake) and the reconstruction algorithms are run again with looser settings, improving the efficiency but keeping the fake rate low. Then a clustering algorithm groups the calorimeter cells into clusters. First cluster seeds are found by searching for maxima in the cluster cells which lie above a certain threshold. Then they are combined into topological clusters by combining all neighbouring cells with the seeds as long as the energy again exceeds a certain threshold. These topological clusters are then separated into particle flow clusters by sharing the energy among the clusters according to the distance between the cells and the cluster itself.

During the second step associations are made between the basic elements. This association is quantified by the distance between the different elements which are extrapolated from one detector part to another. Tracks are extrapolated from their last hit in the tracker to the second layer of the calorimeter and associated to a cluster if the extrapolated position lies within the cluster boundaries. Clusters in the electromagnetic calorimeter can be associated to the ones in the hadronic calorimeter if they also overlap. Finally charged tracks can be extrapolated to the muon systems and combined into a global muon if the

[3]This is mostly a problem for calorimeters.

tracker tracks and the muon system tracks are compatible.

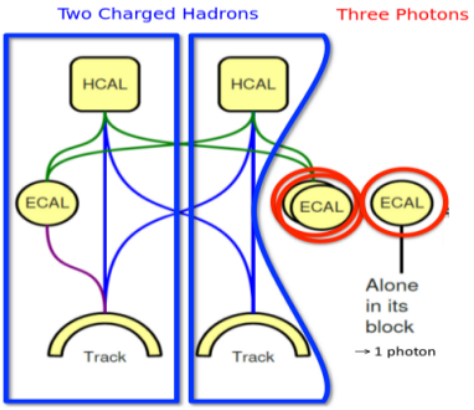

Figure 2: Many associations have been made between the different basic elements. It is the goal of the particle flow reconstruction algorithm to refine these associations and end up with the correct final state particles. [4]

The last step is the particle flow reconstruction algorithm itself. Several associations are made, some of which need to be refined to end up with stable final-state particles (see figure 2). This is done for photons, charged and neutral hadrons (mostly pions) whereas electrons and muons are dealt with in a slightly different way which will be discussed afterwards. First of all, the associations between tracks and clusters are removed until every track is only associated to the closest cluster. Then the energy in the calorimeter clusters[4] is compared to the sum of the energy of all the associated tracks to that cluster and several situation may arise. If the calorimeter energy matches the energy of the tracks, only charged hadrons are identified. If the calorimeter energy is higher than that of the tracks, the charged hadrons are identified by the tracks and their energy removed. The remaining energy is used to construct either photons (especially when there is a lot of energy in the electromagnetic calorimeter) and eventually neutral hadrons. In some cases the energy of the tracks is higher than the calorimeter energy, in which case tracks are removed by looking further for muons or eliminating tracks with high uncertainties.
Electrons and muons are reconstructed separately. No clusters are used, but rather a sliding window algorithm is performed. This includes a search for fixed squares of calorimeter cells in attempt to choose the most optimal one. Furthermore electrons tend to radiate away a lot of bremsstrahlung photons, which also have to be identified by searching for clusters in the electromagnetic calorimeter in a direction tangent to the electron track.
Finally one ends up with a set of final state particles, which can be used for further analysis as for example to construct isolation cones. The main question that arises is whether or not the use of particle flow objects to construct isolation cones may improve the efficiency and the fake rejection. This means the truly isolated particles should be identified, without allowing any non-isolated particles to pass the isolation criteria.

In this note, the possibility for particle flow to improve isolation is investigated. Section 1 includes the technical details of this study, explaining the specific samples and objects that have been used. In section 2, different types of isolation are discussed together with different possible parametrizations for particle flow isolation and the cuts that have been used. In section 3 the pile-up subtraction for charged and neutral particle flow objects is discussed and finally in section 4 there will be a detailed investigation of the efficiency and rejection against fakes, which will be compared to other types of isolation.

[4]The calorimeter energy needs to be precisely calibrated, but a full treatment falls beyond the scope of this paper and can be found in for example [6]

1 Technical Details of this Study

This section describes the particles which were used to study isolation and the samples that were used to achieve this.

1.1 Objects

This study is focused on the isolation of muons. This choice was made since muons have a very clean signature in the detector and do not suffer from a significant contribution from fakes. During this study three types of muons are of interest:

- The signal consists of promptly produced muons from the hard scatter event.
- Background arises from fakes inside jets, which could be due to an in flight decay of a pion or due to punch through into the muon spectrometer.
- Background muons produced from semi-leptonic decays of b-hadrons within jets.

Selection cuts are applied to the muons before constructing isolation cones. This implies cutting on the quality of the reconstructed muon and also on some of its parameters like p_T and η. These cuts could vary between different analyses, depending on the needs and interests of that research. To investigate isolation, one set of cut parameters has been chosen and kept constant during the entire analysis. The cuts used follow the MCP guidelines[5] and are listed below:

- $p_T^\mu > 20$ GeV
- The muon has to be a *combined muon* meaning the reconstruction algorithm which combines the tracker and muon system information was successful.
- Cuts on the impact parameters[6] d_0^{PV} and z_0^{PV}: they must not deviate too much from the position of the primary vertex from which the muon is created: $|d_0| < 0.2mm$ and $|z_0| < 1mm$.
- Number of pixel hits + number of crossed dead pixel sensors > 0
- Number of SCT hits + number of crossed dead SCT sensors > 4
- Number of pixel holes[7] + number of SCT holes < 3.
- Let $nTRT^{hits}$ denote the number of TRT hits on the muon track, $nTRT^{outliers}$ the number of TRT outliers[8] on the muon track, and $n = nTRT^{hits} + nTRT^{outlier}$. Then require $n > 5$ and $nTRT^{outliers} < 0.9 \times n$

Isolation cones will be constructed from charged and neutral particle flow objects. A distinction between charged and neutral objects will be made because they require a different treatment in terms of pile-up subtraction and they also appear in different amounts, making it interesting for isolation to make distinct cuts on charged and neutral objects. There is an intrinsic limitation to the particle flow reconstruction algorithm by the limited η coverage of the inner detector [2]. This means no attempt is made to reconstruct charged particle flow objects with $|\eta| > 2.5$.

[5] https://twiki.cern.ch/twiki/bin/viewauth/AtlasProtected/MCPAnalysisGuidelinesData2012

[6] The transverse impact parameter d_0^{PV} is defined as the distance of closest approach from the track to the primary vertex. The longitudinal impact parameter z_0^{PV} is defined as the distance along the beamline from the primary vertex to the point of closest approach from the track to the beamline.

[7] Holes are missing hits in one of the layers of the tracking system while extrapolating the reconstructed track.

[8] Outliers are hits in the TRT that are not compatible with the reconstructed track taking into account the typical resolution in the TRT.

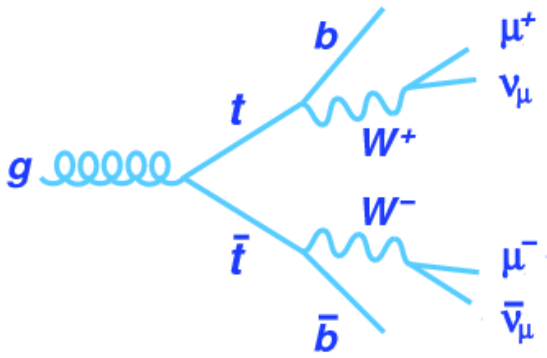

Figure 3: A Feynman diagram describing the creation of a top anti-top pair and the subsequent decay into bottom quarks and leptons. The muons resulting from the W decay will be isolated, but it can also be that muons are created within the b-jets (for example as the result of an in-flight pion decay). Isolation will fail for these muons since they are surrounded by a lot of energy from the b-jet. [7]

1.2 Samples

Three different samples were used throughout the study, all of which are standard 8 TeV samples including pile-up:

- The ttbar sample: simulating top anti-top events. This sample contains prompt isolated muons, resulting from the decay of W boson as shown in figure 3, but it also contains non-isolated muons created in the b-jets and which allows for a comparison between isolation efficiency and fake rejection. This sample was also used for the study and validation of correct pile-up subtraction.
  sample names: *user.cyoung*.019026.*EXTO*._00???.*physics.root*
- The $Z \rightarrow \mu\mu$ sample: simulating pure $Z \rightarrow \mu\mu$ signal events without background events. This sample was used to investigate whether particle flow isolation seemed to work well and for initial studies of the pile-up subtraction. This sample however contained only isolated muons.
  sample names: *user.cyoung*.018557.*EXTO*._00???.*physics.root*
- The JX sample: simulating jets. This sample was used to study background events, which were lacking in the $Z \rightarrow \mu\mu$ sample.
  sample names: *user.cyoung*.017895.*EXTO*._00???.*physics.root*

In all of these samples, the muons are reconstructed by the *staco* algorithm, indicated by prefix *mu_staco_* for all the muon variables. Another muon reconstruction algorithm is available at ATLAS (muid), but as there is not expected to be a strong dependence of isolation on the algorithm, only the staco algorithm has been used throughout this study. The particle flow objects have been given a prefix $eflow\_eflow\_$. From now on, the particle of interest will always be a muon, although similar studies could be done for other particles.

2 Particle Flow Isolation

This section first covers some different types of isolation. After that the concept of relative isolation will be introduced and its use will be justified. Finally a more detailed description of particle flow isolation will be given.

2.1 Different Types of Isolation

As already explained, isolation algorithms construct a cone in η and ϕ around a muon, and gather all energy that falls within the cone. Different types of isolation can be distinguished this way, depending on what objects are used to construct the isolation cones. Previously only tracks or calorimeter cells were used to construct isolation cones. Particle flow isolation uses clusters instead of calorimeter cells together with the tracks. These three types of isolation will be briefly discussed, but similar studies are ongoing, using only clusters for lepton isolation (see for example [8]).

The first type of isolation uses tracks within the inner detector part of the ATLAS detector. Consequently this only implies charged particles since neutral particles don't produce tracks. This type of isolation is already run during reconstruction and available as 'ptcone20, ptcone30 and ptcone40', and will be referred to in the same way throughout this note. The numbers represent the size of the isolation cone, which will be discussed in one of the next sections. In general, charged isolation is much less sensitive to pile-up since it is easier to identify the origin of the tracks.

Then a second type uses energy in the calorimeters. It uses both electromagnetic and hadronic calorimeter cells to construct the isolation cones. Also this isolation type is already run during reconstruction and available as 'etcone20, etcone30 and etcone40', since calorimeter information provides an energy measurement (E_T) whereas the tracks provide a measure of transverse momentum (p_T).

Finally one can use the combined information of all the detector elements and use the particles obtained from the particle flow algorithm to construct an isolation cone. This is exactly the goal of this study and it will be referred to as p-flow isolation.

2.2 Relative Isolation

2.2.1 Definition

Isolation ($\mathfrak{I}$) can be transformed into relative isolation ($\mathfrak{R}$) by taking the ratio with respect to the p_T of the muon. The definition can be found in equation 2.

$$\mathfrak{R} = \frac{\sum p_T(\in cone)}{p_T^{\mu}} \tag{2}$$

2.2.2 Stability against p_T and η

Standard (non-relative) isolation has a large dependence on the pseudorapidity (η) and the p_T of the muon. This is shown in figure 4(a) and 4(c). Isolation is expected to grow with increasing p_T since the muon will radiate away more energy at higher p_T. This radiation may cause showers in the detector and because the muon is boosted these showers will most likely be in almost the same direction as the muon, adding energy to the isolation cone. This effect is far more pronounced when investigating electrons instead of muons since electrons radiate away a lot of bremsstrahlung photons. The η dependence just represents the distribution of matter in the detector.

It would however be far better to make isolation almost independent of these variables, making it possible to use a single p_T- and η independent cut on the isolation. Figure 4(b) and 4(d) show that relative isolation is far more stable (flat) against η and p_T^{μ}, making it the logical choice for parametrizing the isolation cones. At low p_T, there is an increase, but these muons are less critical for physics analyses.

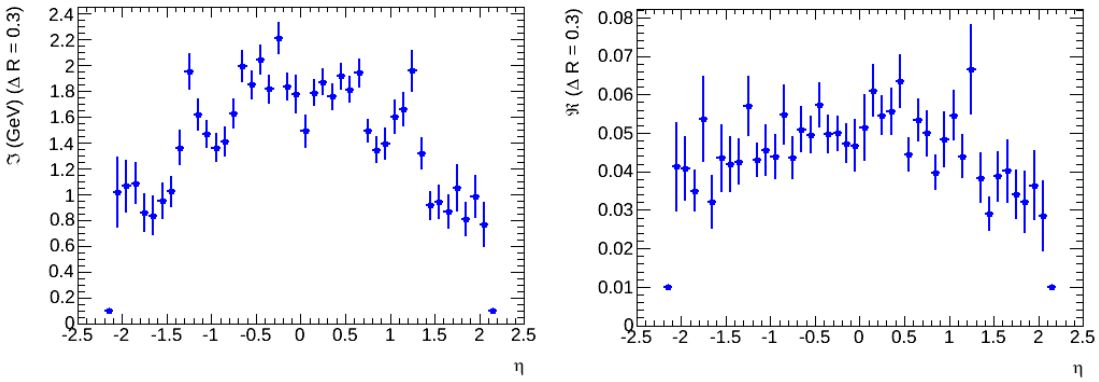

(a) Standard isolation ($\mathfrak{I}$) as a function of η

(b) Relative isolation ($\mathfrak{R}$) as a function of η

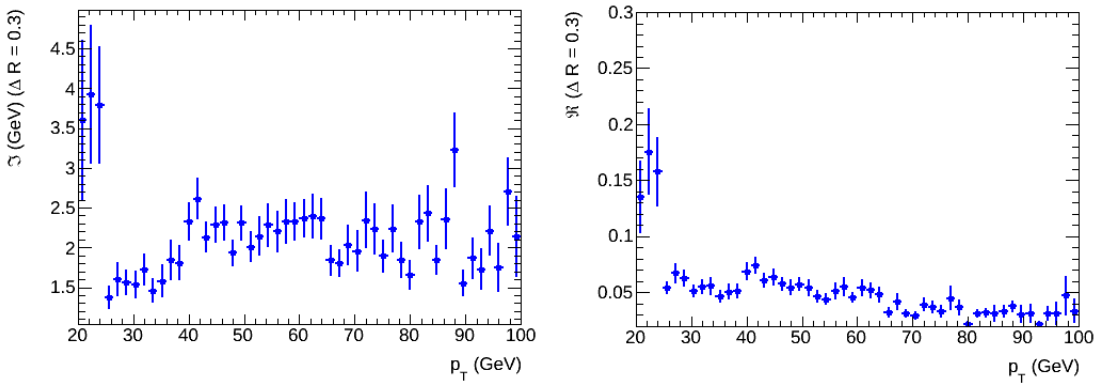

(c) Standard isolation ($\mathfrak{I}$) as a function of p_T^{μ}

(d) Relative isolation ($\mathfrak{R}$) as a function of p_T^{μ}

Figure 4: Comparison of the η and p_T dependence between normal and relative isolation. Sample: ttbar (10000 events).

2.3 Creating Particle Flow Isolation Cones

After selecting the muons using the selection criteria outlined in section 1.1, a selection is applied to the particle flow objects used to construct the isolation cones. Charged and neutral particle flow objects are treated separately throughout the entire process of creating the isolation cone. Besides the intrinsic limitation of the η coverage, only one extra cut is being made concerning the particle flow object transverse momentum: $p_T^{ch} > 1$ GeV and $p_T^{neu} > 0.6$ GeV[9]. Later, when discussing the efficiency and fake rejection, the dependence on the precise value of this cut has also been studied.
Having the selected particle flow objected at hand, the isolation cone can be filled. An isolation cone is defined by its radius in the η-ϕ plane: ΔR, as defined in equation 3. Typical values for ΔR are 0.2, 0.3 and 0.4, which is translated into a suffix 20, 30 or 40 when talking about the different types of isolation. Figure 5 shows the distribution of ΔR for 1000 events in the ttbar sample.

$$\Delta R = \sqrt{\Delta\eta^2 + \Delta\phi^2} \tag{3}$$

Every particle for which $\sqrt{\Delta\eta^2 + \Delta\phi^2} < \Delta R$ is considered to lie within the cone. For charged particles this matching is done at the primary vertex, where η and ϕ are defined by the tangent to the origin of the

[9]This difference between charged and neutral is due to the fact that the neutral energy is calculated from the clusters which are at EM scale. This calibration slightly underestimated the energy.

reconstructed track. Neutral particles are matched at the surface of the calorimeters, where η and ϕ are defined by the reconstructed direction of the clusters inside the calorimeter. This is a bit more subtle, since originally the clusters aim towards a fixed arbitrary point on the beamline and a correction is made in order to deduce the true direction with respect tot he primary vertex of the particle. In equation 3, $\Delta\eta$ ($\Delta\phi$) is the difference in η (ϕ) between the muon around which the cone is constructed and the particle flow object which is considered. By checking this inequality, the isolation cone is filled with charged and neutral particle flow objects.

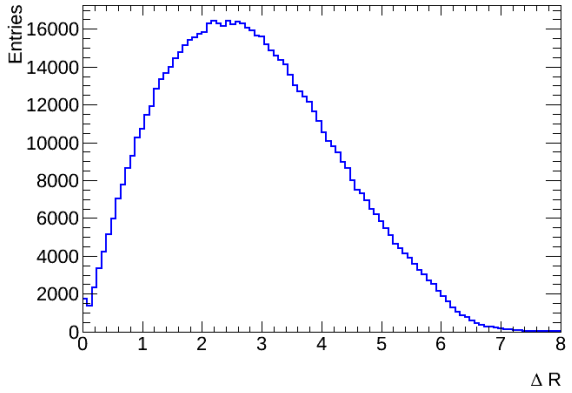

Figure 5: Distribution of ΔR for particle flow objects in 1000 events (signal and background) of the ttbar sample. Only the particles for which ΔR is smaller than the conesize fall inside the cone, but it must not be forgotten that some of them are from pile-up or they could be the muon itself and these still need to be subtracted from the cone.

It is checked that the muon track itself (which can of course also be reconstructed by the particle flow algorithm and lies within the cone by definition) is subtracted from the cone. Secondly the possible pile-up that entered the cone is subtracted. Pile-up subtraction is discussed in section 3. Finally one divides the remaining energy inside the isolation cone by the p_T of the muon to end up with the relative isolation for that muon.

To determine whether or not the muon is isolated, a certain threshold on the relative isolation is chosen. This value will be referred to as the (relative) isolation threshold. Whenever the relative isolation falls below this threshold value, the muon is considered isolated. This value may differ when looking at only charged particles, only neutral particles or a combination of both. The optimization of this threshold value is discussed in section 4.

A comparison was first made to the ptcone and etcone (where for the relative etcone, one uses the muon E_T instead of the p_T), shown in figure 6. A conesize of $\Delta R = 0.3$ has been used. In figure 6(a) the charged and neutral particle flow isolation is compared separately to the ptcone and etcone. In figure 6(b) the nucone30 (number of tracks inside the ptcone30) is compared to the number of charged and neutral particle flow objects in the isolation cone.
From figure 6(a) it is clear that the charged particle flow isolation is very consistent with the ptcone. This is expected because ptcone is based only on tracks as in the charged p-flow cone. The neutral particle flow isolation is more comparable to the cluster based etcone, but falls slightly below it since it contains no information on the charged particles. Additionally etcone has some special corrections [3] which also explains the difference. Photons or electrons might leak some energy in the calorimeters outside of their central core, which might contaminate their isolation cone and which is taken care of by the leakage correction. A second correction to etcone is the pile-up correction, which subtracts an average pile-up energy based on either the number of primary vertices or by calculating an event based pile-up energy density. In figure 6(b) again the similarity between charged particle flow isolation and ptcone shows. The neutral particle flow isolation should however not be compared to any of the other two, since they do not contain information on the neutral objects. Particle flow isolation is largely consistent with other types of isolation, but the main question remains whether it may improve the performance of isolation

in discriminating signal from background. Therefore the subtraction of pile-up and the efficiency of the particle flow isolation will be further studied.

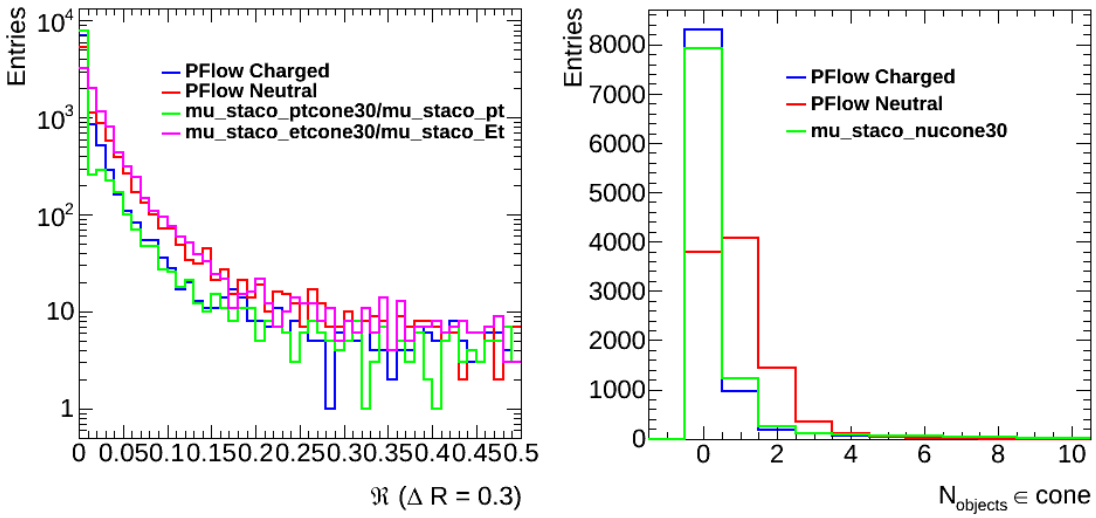

(a) Distribution of $\mathfrak{R}$

(b) Distribution of $N_{objects}$ inside the cone

Figure 6: Comparison between p-flow isolation and ptcone and etcone for signal muons. (a) Distribution of the relative isolation for charged and neutral particle flow isolation separately, which is compared to the track based ptcone and the cluster based etcone. (b) Distribution of the number of particles inside the isolation cone again separately for charged and neutral particle flow objects, which is compared to nucone (number of tracks inside ptcone). Sample: ttbar (10000 events).

3 Pile-Up Subtraction

In equation 3, all energy within an isolation cone is included. Any pile-up particle that is created in a completely different vertex than the one from the muon can still fall inside the isolation cone when it has similar η and ϕ compared to the muon. This is illustrated in figure 7. The same problem arises for out-of-time pile-up, but it might even be more problematic since charged particles from a previous collision can not be identified because the tracks are not present any more. The underlying event probably contaminates the cones even more because those tracks are produced close to the ones from the actual hard scatter. Charged and neutral particles require different pile-up subtraction methods, because of their different signatures in the detector. This section describes the pile-up subtraction used during this analysis and discusses the results.

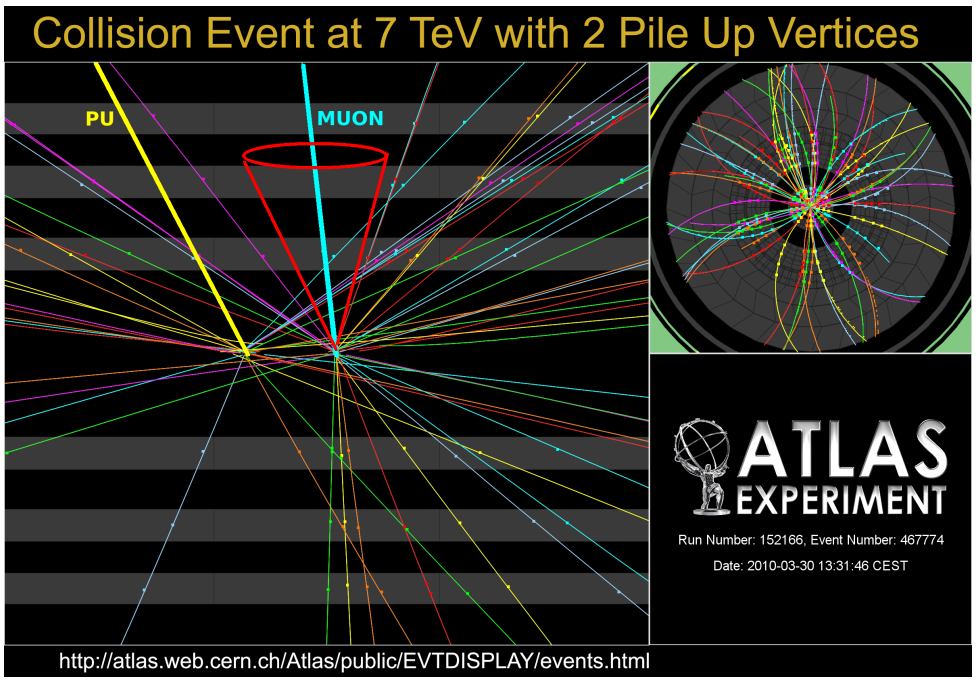

Figure 7: Collision event inside the ATLAS detector at 7 TeV with two pile-up vertices [1]. The yellow pile-up track has similar η and ϕ as the blue muon track, but would not be included in the red isolation cone since it lies far enough from the muon.

3.1 Charged Pile-Up Subtraction

Charged particles produced in pile-up interactions can easily be identified. They leave tracks in the inner detector, which provides information on the position of the primary vertex with a sufficient precision to distinguish different vertices during the same bunch crossing. The position of the track along the beam-line is denoted by the distance z_0 with respect to the middle of the detector. Therefore we can identify the muon by its z_0 position, and any charged track which has its origin far enough from the muon track is considered pile-up.

A new cut is introduced, which will be referred to as the Δz_0 cut. Δz_0 is defined as the distance along the beamline between the z_0 of the muon and the z_0 of the track: $\Delta z_0 = |z_0^{track} - z_0^{\mu}|$. The precise value of the cut depends on the precision with which both of the tracks can be reconstructed and the average distance between two tracks from a different primary vertex. If this precision is higher than the average distance between the two tracks (which it is), it provides a lower bound on the Δz_0 cut and the upper bound is then given by the average distance between tracks from different vertices.
If we consider an average bunch crossing with about 20 vertices spread over 200 mm, we expect approximately a 10 mm spacing between the vertices. This defines the upper limit. The resolution of the reconstructed position of the track is much better and so any value between 1 and 10 mm would be a good cut on Δz_0. This is justified by figure 8, where it is clear that only at very high values of Δz_0 relative isolation starts to become dependent on the number of primary vertices and therefore on the amount of pile-up. During this analysis, different values for Δz_0 were tested and eventually a value of $\Delta z_0 < 3$ mm has been chosen to investigate the efficiency and fake rejection of p-flow isolation. Although other values for this cut work fine as well in term of controlling the pile-up, the isolation efficiency shows a significant dependence on this cut. A cut at 3 mm was chosen to optimize this efficiency.

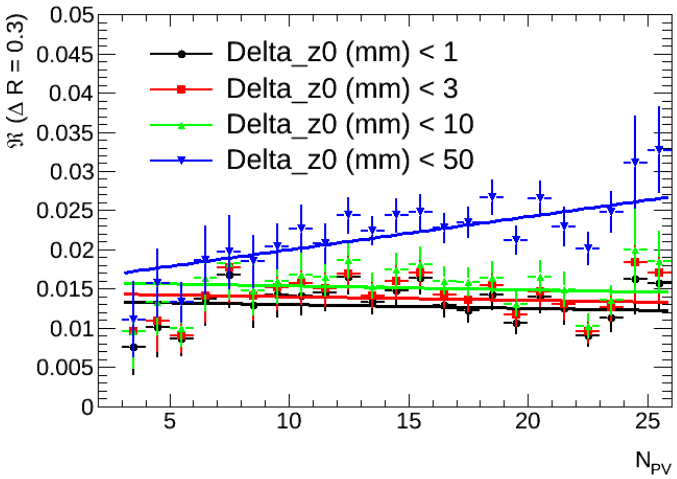

Figure 8: Relative isolation as a function of the number of primary vertices for different Δz_0 cut values. Only when going up to very high values of Δz_0, the pile-Up subtraction starts to fail. Sample: ttbar (10000 events).

3.2 Neutral Pile-Up Subtraction

Removing the contribution from neutral pile-up is more challenging, because neutral particles don't produce tracks and therefore no information on the originating vertex is available. Therefore the idea has been introduced to determine an event-per-event overall neutral pile-up density, called ρ_{neu}. This parameter was calculated using the FastJet software package [11], which originally aims at reconstructing jets. ρ is currently used as a correction applied in jet finding algorithms, but this is the first time it is being used for isolation. All of the neutral particle flow objects were used as an input and the resulting neutral energy density ρ_{neu} can be interpreted as the amount of energy per unit area in the η-ϕ plane. However it must be assumed that all of the neutral particles have a uniform distribution in η and ϕ. Multiplying this parameter by the area of the isolation cone[10] provides an estimate of the neutral pile-up energy inside the isolation cone, as expressed in equation 4.

$$PU_{neu} = \rho_{neu} \cdot \pi \cdot \Delta R^2 \tag{4}$$

Since ρ_{neu} is an average value, a larger spread is expected on the accuracy of the neutral pile-up subtraction. However it is currently the best measure and as will be shown in the next section, on average it seems to give reliable results.

3.3 Results

To check whether the pile-up subtraction (both neutral and charged) is working properly, the dependence of the relative isolation on the number of primary vertices (N_{PV}) in the event was studied for signal muons. The number of primary vertices provides a good estimate of the amount of pile-up in the event, and so ideally we would like relative isolation not to be dependent on the pile-up any more. Figure 9 shows this dependency for charged and neutral particles, before and after the pile-up subtraction and for different conesizes.

[10]This area is again defined in the η-ϕ plane: $A_{cone} = \pi \times \Delta R^2$

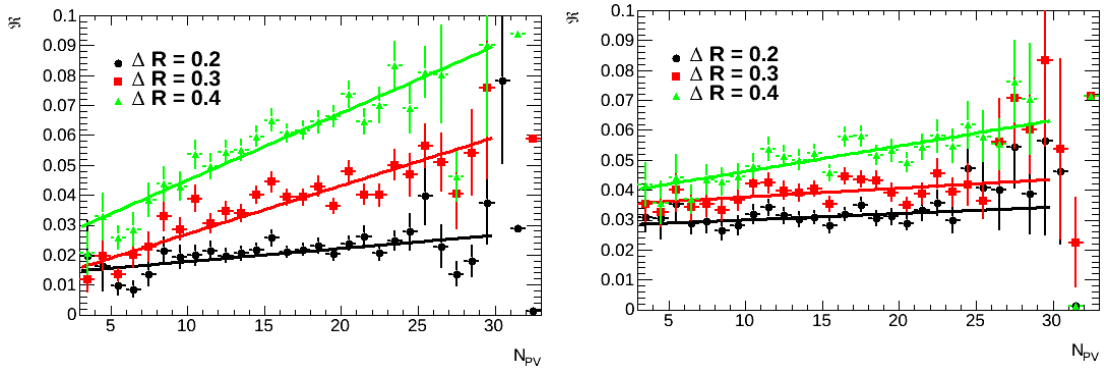

(a) Charged p-flow objects before pile-up subtraction

(b) Neutral p-flow objects before pile-up subtraction

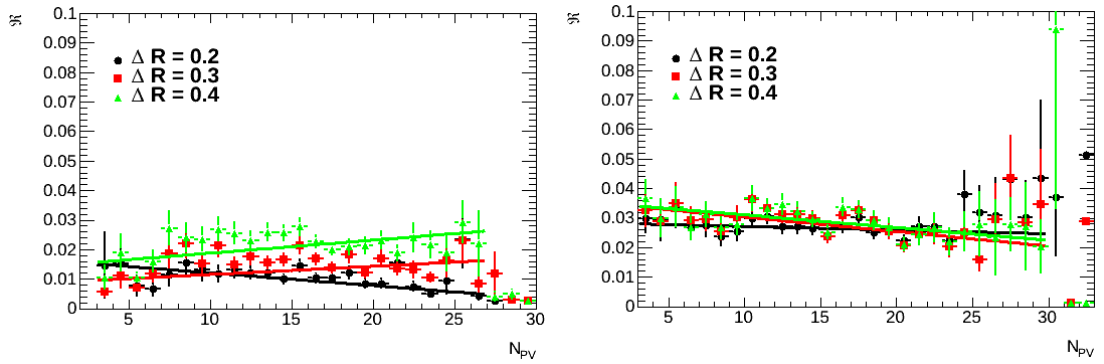

(c) Charged p-flow objects after pile-up subtraction

(d) Neutral p-flow objects after pile-up subtraction

Figure 9: Relative isolation as a function of the number of primary vertices and for different conesizes for signal muons. Sample: ttbar (10000 events).

The larger the isolation cone, the more pile-up is being reconstructed inside it. This fact together with the expected rising behaviour before pile-up subtraction indeed shows in figure 9(a) and 9(b). After pile-up subtraction, figures 9(c) and 9(d) clearly show that relative isolation is almost independent of pile-up, but also much less dependent on the conesize. This indicates that on average the pile-up subtraction is efficient, since isolation is not influenced by the amount of pile-up and is almost independent of the conesize which is used.

4 Isolation Efficiency vs. Fake Rejection

The ideal isolation would pick out all truly isolated muons, but without allowing any non-isolated muons to pass the isolation criteria. A truly isolated muon that is identified as such by the particle flow isolation algorithm will be called a *real*, whereas a non-isolated muon that passes the isolation criteria will be called a *fake*. In order to quantify the quality of isolation, two quantities will be introduced: the isolation efficiency and the fake rejection. These quantities will express how well isolation identifies the truly isolated muon and how well it eliminates fakes. In general it is hard to find out which muons are truly the isolated ones, but the truth information from Monte Carlo simulated samples provides some information.

4.1 Definitions

Truth-isolation A fiducial definition of isolation is introduced where isolation is calculated at the truth level using the same algorithm as particle flow isolation, but using the truth-particles from the Monte Carlo simulation to fill the isolation cone instead of the reconstructed particle flow objects. A status code of 1 is used to identify the final stable simulated particles. Also the conesize is kept high and constant at a value of $\Delta R^{truth} = 0.4$, while the (relative) isolation threshold[11] is kept relatively low and constant at a value of $\mathfrak{R}^{truth} = \mathfrak{R}^{truth}_{ch} + \mathfrak{R}^{truth}_{neu} < 0.05$. This large conesize with a small threshold ensures the truth isolation is quite pure, in the sense that it will allow only a few fakes. Also the pile-up subtraction for the neutrals is different, since the neutral truth particles contain information on the primary vertex they came from, making it possible to also apply a Δz_0 cut on the neutrals.
This definition of truth isolation allows for a comparison between different kinds of isolation as will be discussed in the next section. Therefore it will be of interest whether a particle that is truth isolated, is also found to be isolated by other types of isolation and which type of isolation has the highest efficiency and fake rejection.

Efficiency and fake rejection Efficiency (ϵ) and fake rejection (R) are defined in equations 5 and 6. In these definitions, N^{fake} are particles that are not truth isolated but are found to be particle flow isolated, whereas N^{real} are both truth and particle flow isolated. Let N^{truth}_{iso} denote the total number of truth isolated muons (signal) and $N^{truth}_{non\_iso}$ denote the total number of truth non-isolated muons (background).

$$\epsilon = \frac{N^{real}}{N^{truth}_{iso}} \tag{5}$$

$$R = 1 - \frac{N^{fake}}{N^{truth}_{non\_iso}} \tag{6}$$

Using these definitions, the efficiency is 1 when all of the truth isolated muons are indeed found to be particle flow isolated and the fake rejection goes up to 1 when there are no fakes.

Tight, medium and loose isolation Efficiency and fake rejection are inversely correlated. Therefore optimisation requires balancing conflicting requirements. In order to compare different types of isolation, three definitions have been introduced to define the efficiency and the isolation threshold that is needed to reach it[12]. Tight isolation uses the tightest isolation threshold meaning it has the lowest efficiency, but ensures the highest fake rejection. Loose isolation is the opposite, yielding the highest efficiency, but the lowest fake rejection and medium provides a balance between the two. Table 1 shows the three efficiencies chosen in the three cases.

Table 1: The efficiency for the three definitions of isolation.

Isolation definition	Required efficiency
Tight	0.85
Medium	0.90
Loose	0.95

[11] In the truth-isolation the charged and neutral relative isolation is added together and the isolation threshold is applied to the sum of both.

[12] A lower isolation threshold implies a tighter cut and therefore a lower efficiency, but a higher fake rejection

4.2 Results

The information from p-flow isolation techniques can be combined in a number of different ways. As particle flow contains information on both charged and neutral objects, four categories are distinguished:

- Using only charged particle flow objects
- Using only neutral particle flow objects
- Using both charged and neutral particle flow objects, adding their relative isolation together and defining an isolation threshold on the sum of both. This will be referred to as the 1D cut.
- Using both charged and neutral particle flow objects and putting and isolation threshold on each of them separately. This will be referred to as the 2D cut.

Each of these will now be discussed and compared to ptcone and etcone. The resulting plots, showing efficiency and fake rejection for different isolation threshold values, are found in figure 11. A validation for the used threshold values can be found in figure 10, where the correlation between neutral and charged relative isolation is shown for signal (left) and background (right). Cutting on charged and neutral isolation (2D cut) is equivalent to cutting out a square in this plane. More complex cuts might prove to be even more effective.

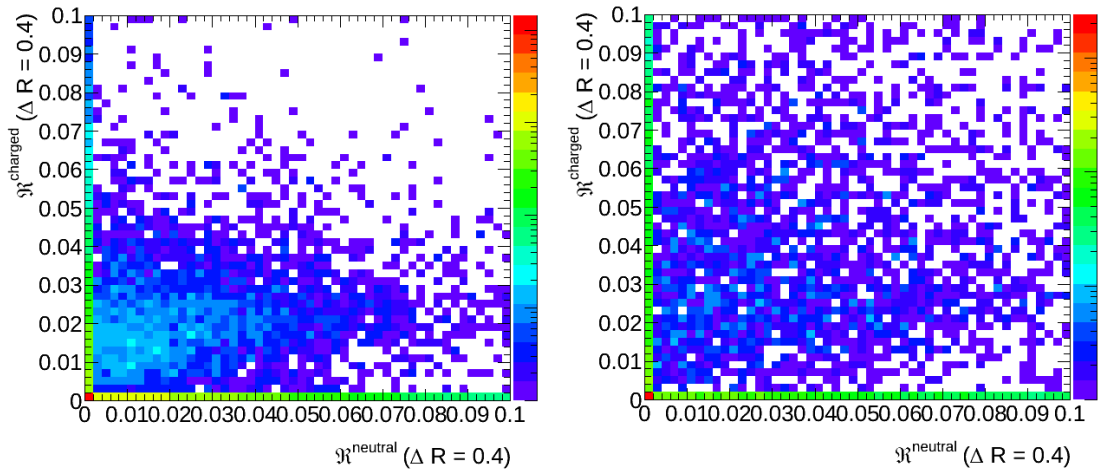

(a) Signal (b) Background

Figure 10: Correlation between the neutral and charged relative particle flow isolation for signal (a) and background (b). Sample: ttbar (67510 events)

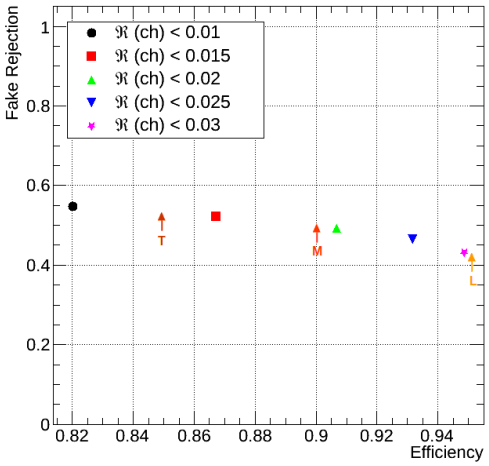

(a) Only charged particle flow objects

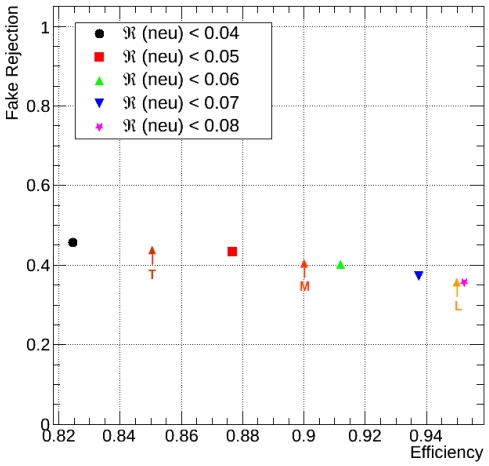

(b) Only neutral particle flow objects

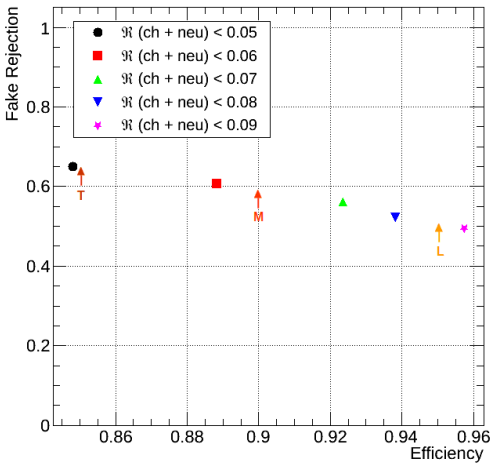

(c) Charged and neutral particle flow objects (1D cut)

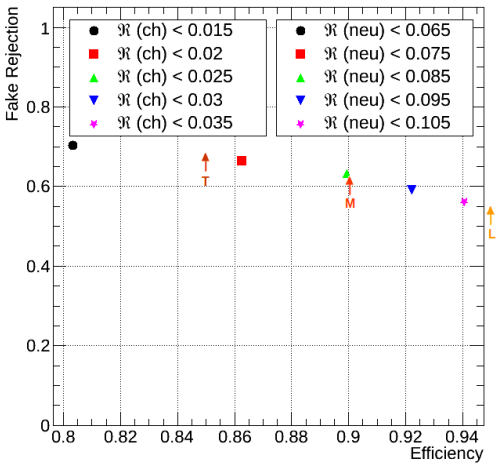

(d) Charged and neutral particle flow objects (2D cut)

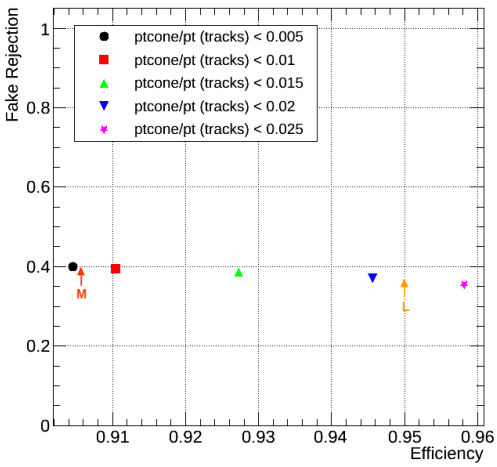

(e) ptcone: only tracks

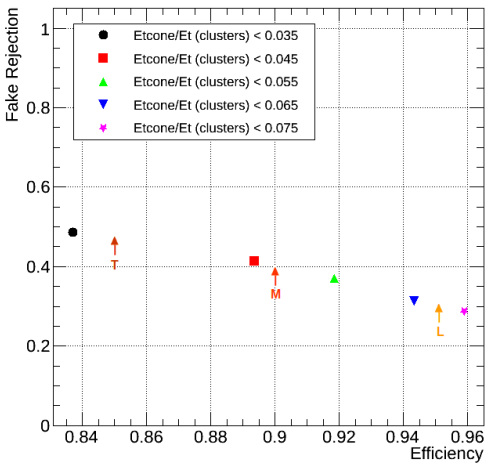

(f) etcone: only calorimeter cells

Figure 11: Comparison of isolation ($\Delta R = 0.4$) efficiency vs. fake rejection for different types of isolation and for different values of the isolation threshold. The three definitions of isolation: Tight (T), Medium (M) and Loose (L) are indicated by arrows with the corresponding letter. Sample: ttbar (2000 events)

Only Charged The efficiency and fake rejection for different isolation threshold values using only charged particle flow objects is shown in figure 11(a). The value of the fake rejection and isolation threshold for the three definitions of isolation are given in table 2.

Table 2: Fake rejection and isolation threshold for the three definitions of isolation using charged particle flow objects.

Isolation definition	Required efficiency	Fake rejection	Isolation threshold (ch)
Tight	0.85	0.53	0.015
Medium	0.90	0.50	0.02
Loose	0.95	0.44	0.03

Only Neutral The efficiency and fake rejection for different isolation threshold values using only neutral particle flow objects is shown in figure 11(b). The value of the fake rejection and isolation threshold for the three definitions of isolation are given in table 3.

Table 3: Fake rejection and isolation threshold for the three definitions of isolation using neutral particle flow objects.

Isolation definition	Required efficiency	Fake rejection	Isolation threshold (neu)
Tight	0.85	0.44	0.045
Medium	0.90	0.40	0.06
Loose	0.95	0.35	0.08

Charged and Neutral (1D cut) The efficiency and fake rejection for different isolation threshold values using both charged and neutral particle flow objects and putting a threshold on the sum of their relative isolation (1D cut), is shown in figure 11(c). The value of the fake rejection and isolation threshold for the three definitions of isolation are given in table 4.

Table 4: Fake rejection and isolation threshold for the three definitions of isolation using the sum of charged and neutral particle flow isolation (1D cut).

Isolation definition	Required efficiency	Fake rejection	Isolation threshold (ch + neu)
Tight	0.85	0.65	0.05
Medium	0.90	0.58	0.065
Loose	0.95	0.50	0.085

Charged and Neutral (2D cut) The efficiency and fake rejection for different isolation threshold values using both charged and neutral particle flow objects and putting a threshold on each of them separately (2D cut), is shown in figure 11(d). The value of the fake rejection and isolation threshold for the three definitions of isolation are given in table 5.

Table 5: Fake rejection and isolation threshold for the three definitions of isolation cutting on charged and neutral particle flow isolation separately (2D cut).

Isolation definition	Required efficiency	Fake rejection	Isolation threshold	Charged	Neutral
Tight	0.85	0.67		0.020	0.075
Medium	0.90	0.63		0.025	0.085
Loose	0.95	0.54		0.035	0.105

Track Based: ptcone The efficiency and fake rejection for different isolation threshold values using only tracks (ptcone) is shown in figure 11(e). The value of the fake rejection and isolation threshold for the three definitions of isolation are given in table 6. The tight definition could not be reached since the (relative) isolation is very often equal to zero, making it impossible to lower the efficiency by lowering the threshold value.

Table 6: Fake rejection and isolation threshold for the three definitions of isolation using tracks (ptcone).

Isolation definition	Required efficiency	Fake rejection	Isolation threshold (tracks)
Tight	0.85	$\backsim$0.40	< 0.005
Medium	0.90	0.40	0.005
Loose	0.95	0.37	0.020

Calorimeter Cell Based: etcone The efficiency and fake rejection for different isolation threshold values using only calorimeter cells (etcone) is shown in figure 11(f). The value of the fake rejection and isolation threshold for the three definitions of isolation are given in table 7.

Table 7: Fake rejection and isolation threshold for the three definitions of isolation using calorimeter cells (etcone).

Isolation definition	Required efficiency	Fake rejection	Isolation threshold (calorimeter cells)
Tight	0.85	0.47	0.035
Medium	0.90	0.40	0.045
Loose	0.95	0.33	0.065

Comparison between the different isolation types A first thing to mention is that the overall fake rejection is rather low, ranging between 40 and 67 percent for the tight definition [13]. This is confirmed by figure 10, where it can be seen that there isn't a very clear distinction between signal and background. Therefore to reach the required efficiencies, still a lot of background falls below the isolation threshold. A discussion on what may cause the fakes is given in the next section.
Figure 12 shows the difference between the different types of isolation for the three isolation definitions. Using only either charged or neutral objects gives quite low fake rejections, going not higher than 0.53 (tight) for charged particle flow objects, but being even worse for neutral objects, limited at 0.44 (tight). The strength of particle flow isolation seems to lay in the fact that you can use both charged and neutral objects. Using a 2-dimensional cut on charged an neutral separately gives the highest overall fake rejection, going up to 0.67 for the tight definition. This appears to be the best parametrization for particle flow isolation.
Even more important is the comparison to etcone and ptcone. It is clear that none of them can reach

[13] All of the following conclusions are applicable to all definitions of isolation (tight, medium and loose).

as high as the (2D) particle flow isolation, going only up to about 0.40 (ptcone) and 0.47 (etcone) for the tight definition. This is a first indication that particle flow isolation does indeed show improvements compared to the already existing ptcone and etcone. Furthermore, the charged p-flow isolation seems to do better on its own than the track based ptcone. This may be caused by the different cuts on the tracks an perhaps by the applied pile-up subtraction.

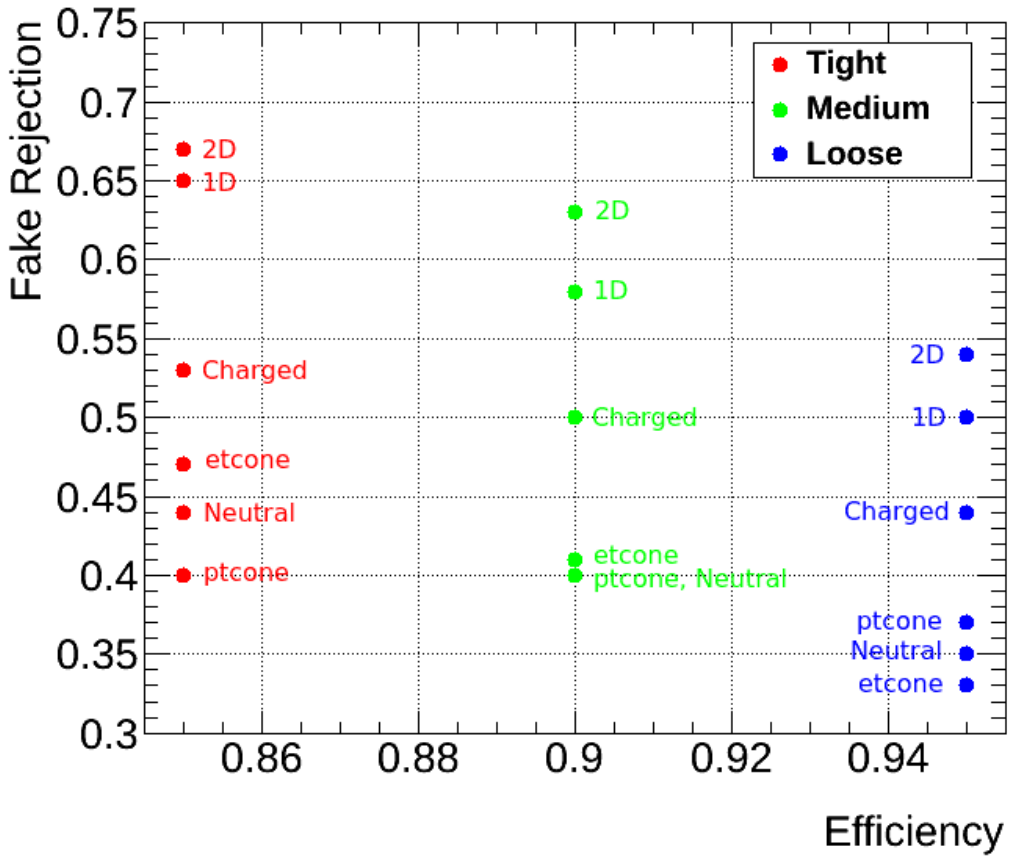

Figure 12: Overview of the efficiency and fake rejection for the three isolation definitions and for the different types of isolation.

Comparison between different cuts on the particle flow p_T The previous results are based on a p_T cut on the particle flow objects: $p_T^{ch} > 1$ GeV and $p_T^{neu} > 0.6$ GeV. However this cut can also be varied and in figure 13 the dependency of the efficiency and fake rejection on this cut is checked. There is only a small dependence on this cut.

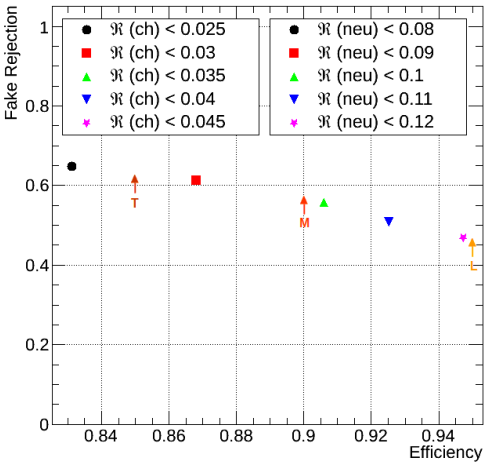

(a) $p_T^{ch} > 0$ GeV and $p_T^{neu} > 0$ GeV

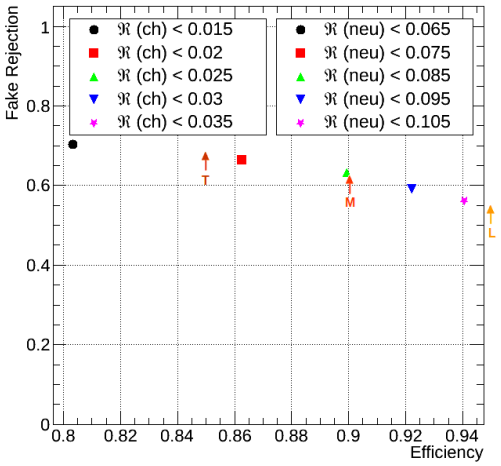

(b) $p_T^{ch} > 1$ GeV and $p_T^{neu} > 0.6$ GeV

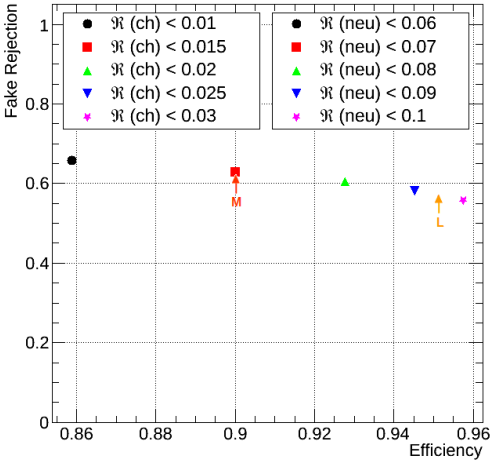

(c) $p_T^{ch} > 2$ GeV and $p_T^{neu} > 1.2$ GeV

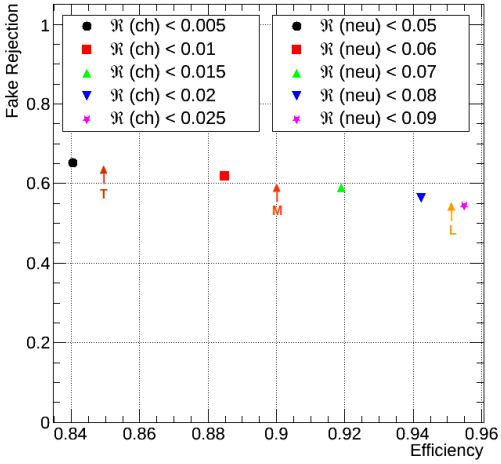

(d) $p_T^{ch} > 3$ GeV and $p_T^{neu} > 1.8$ GeV

Figure 13: Comparison of isolation ($\Delta R = 0.4$) efficiency vs. fake rejection for different cuts on the particle flow p_T. All of these plots use the tight 2D cut for the isolation threshold. Sample: ttbar (2000 events)

4.3 Investigation of the Fakes

As seen in the efficiency and fake rejection plots, the overall fake rejection is quite poor. Therefore a better understanding of where these fakes come from and how they might be avoided is needed. Fakes are caused by a lack of energy (or particles) in the particle flow isolation with respect to the truth isolation. This lack of energy causes them to become particle flow isolated, although the truth isolation contained enough energy to make them non-isolated. Therefore it is of interest to look at the difference between the particle flow isolation energy and the truth isolation energy, and do the same for the number of particles inside the cone. This can be done for charged and neutral particles separately, and the results are shown in figure 14.

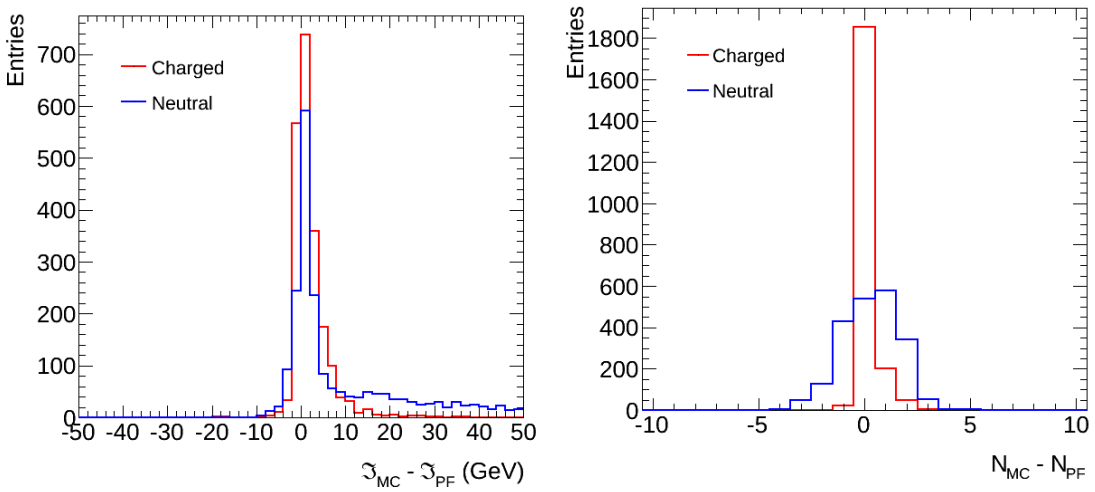

(a) $\Delta\Im$ (b) ΔN

Figure 14: (a) Difference between the truth isolation energy and the particle flow isolation energy for fakes (charged and neutral separately). (b) Difference between the number of particles in the truth isolation cone and the particle flow isolation cone for fakes (charged and neutral separately). In both plots a particle flow isolation conesize of $\Delta R = 0.4$ and the tight 2D isolation definition was used (see table 5). Sample: ttbar (20000 events)

For most of the fakes the energy is underestimated by the particle flow isolation, both for charged and neutral objects. For charged, the number of particles is sometimes underestimated by particle flow, although only by one or two particles and most of the time it even gets the number of charged particles right. For neutrals it appears that particle flow sometimes takes more neutral particles than the truth isolation, but not too much energy. This is however an artefact from the neutral pile-up subtraction. A p-flow object that is added to the isolation cone is identified as a neutral particle if the p-flow charge is 0. These may also include neutral pile-up particles, which have to be excluded by the neutral pile-up subtraction. However, ρ_{neu} is only capable of subtracting an average energy, but has no information on how many particles that energy represents. Therefore the neutral pile-up subtraction for particle flow does not subtract particles (only energy), whereas the truth isolation (which used a Δz_0 cut for the neutrals also) does. This is however not an issue, since isolation relies only on the energy inside the cone, and not on the number of particles that energy represents. Now the charged and neutral fakes can be looked at in more detail.

4.3.1 Charged Contribution to the Fakes

When looking at fakes, the charged component seems quite reliable. Most of the time the number of particles matched those of the truth isolation and the energy doesn't deviate more than 5 GeV. In some cases however one or two particles are lost is particle flow isolation (w.r.t. truth isolation), and the corresponding lost energy is higher. These missing tracks may have two different origins:

- The track was not reconstructed, which can either be caused by the fact that the charged particle had hadronic interactions in the tracker, or because of the tracking efficiency, which is only 87% at a p_T of 3 GeV [9].
- The track was reconstructed, but the particle flow algorithm has its direction slightly off, making

it fall outside of the isolation cone.

To determine which of the above is dominant, the (charged) truth particles inside the isolation cone are matched to the ones in the particle flow isolation cone. This was done by matching the p_T, η and ϕ of the truth particles to those of the particle flow objects[14]. Figure 15 shows that if a truth track was found that did not match any particle flow track inside the cone, it was either because it could be matched to no particle flow track at all (denoted by 0) or it was matched to a particle flow track outside the isolation cone (denoted by 1). In the former case the track reconstruction presumably failed, in the latter case the particle flow algorithm reconstructed the track with a slightly different direction, making it fall outside of the isolation cone.

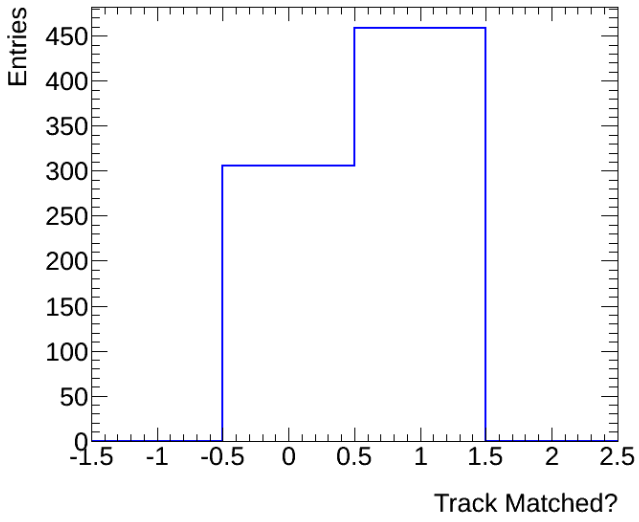

Figure 15: Track matching between truth tracks and particle flow tracks. If a truth track inside the truth isolation cone is not matched to a p-flow track in the p-flow isolation cone, it can either be matched to one outside the isolation cone (1) or to no particle flow track at all (0). A particle flow isolation conesize of $\Delta R = 0.4$ and the tight 2D isolation definition were used (see table 5). Sample: ttbar (50000 events).

It is seen that both effects are important. To get a better understanding of the missing tracks (0), they were investigated a bit closer by looking at their dependence on η, the p_T of the muon, the p_T of the track itself and the relative track p_T w.r.t. the muon p_T (p_T^{track}/p_T^{μ}). Figure 16 shows that the η dependence follows the inner detector geometry, slightly peaking at $|\eta| \simeq 1.5$ where the inner detector has the most material and interactions inside the tracker are most likely. Furthermore the occurrence of fakes because of missing tracks happens more often for low p_T muons, caused by the fact that relative isolation is used and a low p_T track that is missing has a bigger effect on the relative isolation of a low p_T muon than on that of a high p_T muon. Most of the missing tracks have their p_T between 1 and 2 GeV which is only a tiny fraction (about 5 percent) of the muon p_T.

[14]The difference in p_T should be smaller than 200 MeV and the difference in η and ϕ smaller than 0.01. If more than one particle matches these criteria the one with the closest p_T is taken.

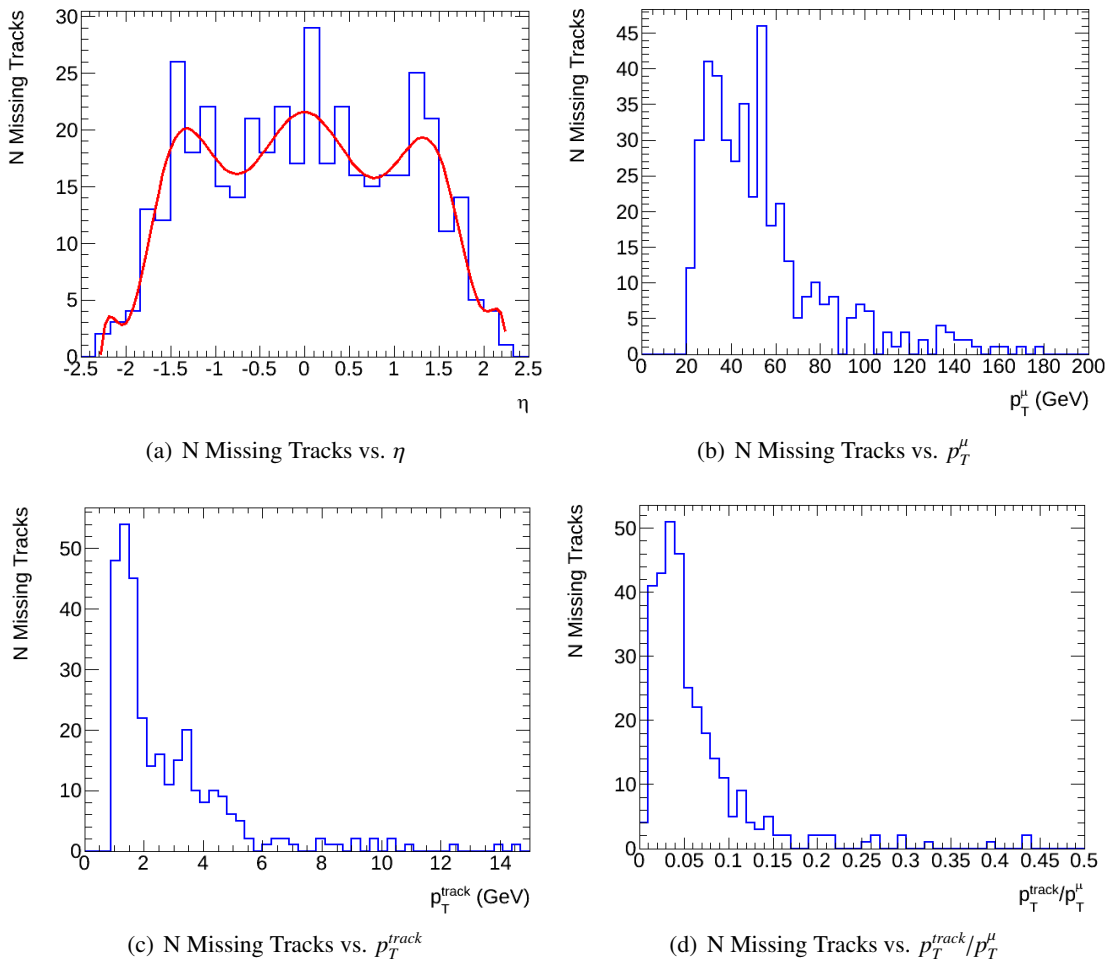

(a) N Missing Tracks vs. η

(b) N Missing Tracks vs. p_T^{μ}

(c) N Missing Tracks vs. p_T^{track}

(d) N Missing Tracks vs. p_T^{track}/p_T^{μ}

Figure 16: Number of missing tracks for fakes as a function of η (a), p_T^{μ} (b), p_T^{track} (c) and p_T^{track}/p_T^{μ} (d). A particle flow isolation conesize of $\Delta R = 0.4$ and the tight 2D isolation definition were used (see table 5). Sample: ttbar (67510 events)

4.3.2 Neutral Contribution to the Fakes

The neutral contribution to the fakes is harder to investigate, and the only parameter currently at hand is the neutral pile-up subtraction (ρ_{neu}). This subtraction may produce fakes, since this amount of energy is always subtracted even if no neutral pile-up was actually present in the cone. Figure 17 shows how many of the fakes would become non-fake if the neutral pile-up subtraction is left out and it can be seen that this does not seem to happen very often.

However, the neutral pile-up subtraction using the ρ_{neu} parameter might not be the best choice after all, and new ideas are being investigated. If for example there is a strong correlation between charged and neutral pile-up in an event, the information of charged pile-up (which is quite well known) could give an estimate of the neutral pile-up. This method would however only work for in-time pile-up.

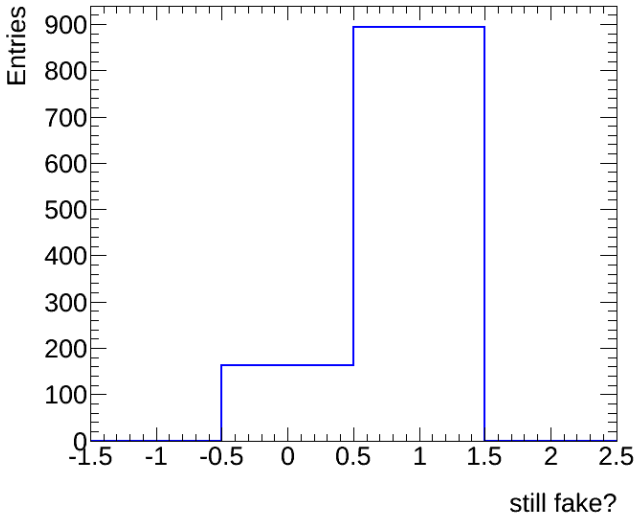

Figure 17: The amount of fake muons that are still fakes without the neutral pile-up subtraction ρ_{neu} (1) compared to the ones that are not fake anymore (0). A particle flow isolation conesize of $\Delta R = 0.4$ and the tight 2D isolation definition were used (see table 5). Sample: ttbar (10000 events).

5 Conclusion and Future Work

The particle flow algorithm combines the information from all the detector elements to construct the stable particles inside the detector. This allow to identify both charged and neutral particles and may be used to improve lepton isolation. Figure 6 shows that particle flow isolation is consistent with previously used track and calorimeter based isolation. Relative isolation is flat with respect to η and p_T, which allows the use of a single threshold on the relative isolation, not depending on these parameters (see figure 4).

The subtraction of pile-up particles from the isolation cone happens differently for charged and neutral particle flow objects. For charged objects a Δz_0 cut discriminates against pile-up tracks from a different primary vertex than the one of the muon. Figure 8 shows that any Δz_0 cut between 1 and 10 mm serves as a good cut and $\Delta z_0 < 3$mm has been chosen to investigate the isolation efficiency and fake rejection. For neutral objects an average pile-up density ρ_{neu} is used to subtract an expected amount of neutral pile-up energy from the isolation cone. Figure 9 shows that this pile-up subtraction makes particle flow isolation on average independent of the amount of pile-up, for different conesizes.

A 2D isolation threshold on charged and neutral p-flow isolation gives the best isolation efficiency and fake rejection. Its results are better than those of the track and calorimeter cell based isolations, which is a first indication that particle flow isolation indeed shows improvements. For the medium isolation definition, p-flow isolation reaches a fake rejection of up to 63% whereas ptcone and etcone both only reach up to 40% fake rejection.

This report has demonstrated that p-flow based isolation can be used to significantly improve performance compared to the traditional isolation types. It improves the fake rejection by more than 20 % for a similar efficiency and makes the isolation on average independent of the amount of pile-up. The next step would be to validate the performance of this algorithm within the context of physics analyses.

Acknowledgments

First of all I would like to thank my supervisors Heather Gray and Andreas Salzburger for giving me the opportunity and trust to complete this research project. They have been providing me with answers and help whenever needed, and all of this always on a very short notice. Further gratitude goes towards Christopher Young for supplying me with all the necessary samples (and explanation about them), and towards all of the members of the particle flow group from ATLAS who helped me with their comments and ideas at the group meetings.

References

[1] ATLAS Collaboration, internet, *http://www.atlas.ch/photos/events-collision.html*

[2] ATLAS Collaboration, *The ATLAS Experiment at the CERN Large Hadron Collider*, 2008 JINST 3 S08003, 14th August 2008

[3] ATLAS Collaboration, *https://twiki.cern.ch/twiki/bin/viewauth/AtlasProtected/CaloIsolationCorrections*, *Calorimeter Isolation Corrections*

[4] C. Bernet, *Particle Flow in CMS: The Data Challenge*, CERN Detector Seminar, 23th september 2011

[5] C. Brust, I. Anderson, P. Maksimovic, A. Sady, P. Saraswat, M. T. Walters, Y. Xin, *Discover New Physics With Non-Isolated Leptons*, BOOST2014, University College London, 18th Aug 2014

[6] CMS Collaboration, *ParticleFlow Event Reconstruction in CMS and Performance for Jets, Taus, and* E_T^{miss}, CMS PAS PFT-09-001, 28th April 2009

[7] Fermilab Collaboration, *Combination of the top-quark mass measurements from the Tevatron collider*, FERMILAB-PUB-12-336-E, arXiv:1207.1069 [hep-ex], 16th November 2012

[8] H. Kajiwara, *Studies of calorimetric isolation for muons using topological clusters*, Muon and Tracking CP meeting in *P&P* week, 3rd September 2014

[9] K. Hamano, A. Morley, A. Salzburger, *Track Reconstruction Performance and Efficiency Estimation using different ID geometry samples*, ATLAS internal note: ATL-COM-PHYS-2012-1541, 25th October 2012

[10] LHC Collaboration, LHC homepage *http://home.web.cern.ch/topics/large-hadron-collider*

[11] M. Cacciari, G.P. Salam, G. Soyez, *FastJet Release 3.0.6*, EPJC72(2012)1896 [arXiv:1111.6097]